ORIGINAL PAPER

A structural bio-chemo-mechanical model for vascular smooth muscle cell traction force microscopy

Shannon M. Flanary[1] · Victor H. Barocas[2]

Abstract

Altered vascular smooth muscle cell (VSMC) contractility is both a response to and a driver for impaired arterial function, and the leading experimental technique for quantifying VSMC contraction is traction force microscopy (TFM). TFM involves the complex interaction among several chemical, biological, and mechanical mechanisms, making it difficult to translate TFM results into tissue-scale behavior. Here, a computational model capturing each of the major aspects of the cell traction process is presented. The model incorporates four interacting components: a biochemical signaling network, individual actomyosin fiber bundle contraction, a cytoskeletal network of interconnected fibers, and elastic substrate displacement due to cytoskeletal force. The synthesis of these four components leads to a broad, flexible framework for describing TFM and linking biochemical and biomechanical phenomena on the single-cell level. The model recapitulated available data on VSMCs following biochemical, geometric, and mechanical perturbations. The structural bio-chemo-mechanical model offers a tool to interpret TFM data in new, more mechanistic ways, providing a framework for the evaluation of new biological hypotheses, interpolation of new data, and potential translation from single-cell experiments to multi-scale tissue models.

1 Introduction

Cell contractility is a fundamental biological phenomenon, arising in processes as diverse as wound healing (Vedula et al. 2015), morphogenesis (Guglielmi et al. 2015), cardiac function (Ross 1983; Saucerman et al. 2003), peristalsis (Singh et al. 2021; Lang et al. 2006), and vasoconstriction (Uehata et al. 1997; Seasholtz et al. 2001). The last example is dominated mechanically by vascular smooth muscle cells (VSMCs), and aberrant VSMC behavior is associated with numerous diseases. Cardiovascular disease is inextricably linked to socioeconomic, environmental, and health behavioral factors, but the underlying etiology involves changes in VSMC contractility within blood vessels (Sun et al. 2015; Brozovich et al. 2016). For example, increased

VSMC contractility, independent of additional factors, leads to hypertension (Uehata et al. 1997; Seasholtz et al. 2001). The underlying mechanobiology that drives the perturbed contractile behavior has been widely studied (Rensen et al. 2007; Irons and Humphrey 2020; Seasholtz et al. 2001), revealing vital knowledge of the various biochemical and mechanical signals that govern the cellular response. Although several factors that can lead to hypertension are often observed in one patient, current analysis and predictions of how such factors interact is not possible.

To analyze cellular mechanobiology experimentally, techniques require both high spatiotemporal resolution and the flexibility to generate meaningful results from a variety of contexts. Thus, traction force microscopy (TFM) has become the prevalent technique to assess the mechanical interface between the cell and the underlying substrate (Schwarz and Soiné 2015). TFM usually involves 2D characterization of cells that have been plated on thin polymer films doped with embedded fluorescent beads. The position of the fluorescent beads while the system is experiencing cell contractile forces is compared to that of the cell-free system, and the resulting displacements can be translated into a traction force since the substrate mechanics are known (Butler

✉ Victor H. Barocas
baroc001@umn.edu

1   Department of Chemical Engineering & Materials Science, University of Minnesota, Minneapolis, MN 55455, USA

2   Department of Biomedical Engineering, University of Minnesota, Nils Hasselmo Hall, Room 7-115, 312 Church St SE, Minneapolis, MN 55455, USA

et al. 2001). TFM has been used to explore the relationship between traction force and focal adhesion contact size (Balaban et al. 2001; Goffin et al. 2006), extracellular stiffness sensitivity in spreading and migration (Trichet et al. 2012), and stem cell differentiation (Wen et al. 2014).

While TFM provides useful information about single-cell behavior, translation to the tissue scale remains difficult without an accurate in silico model. The cell contractile force measured in TFM involves a complex interplay among biological, chemical, and mechanical processes, all of which must be considered to capture the cell's behavior fully. Additionally, the adaptability of TFM has led to the experiment to be used in a variety of contexts, including genetic perturbations, varying micropatterned geometries, and substrate stiffnesses (Porter et al. 2020; Win et al. 2017; Huynh et al. 2013). The interactions and ensuing outcomes throughout the tissue cannot be predicted when multiple perturbations are present by simply combining the results of two independent experiments. A computational model that captures the interconnections between biological, chemical, and mechanical processes in cellular contractility presents the unique capability to bridge the gap between single-cell experiments and that of tissue-level behavior.

Previous in silico models of TFM have ignored the complex biochemical signaling that leads to contractile force generation, and instead simplify the intracellular signaling to a black box (Deshpande et al. 2006). The engagement of myosin onto actin fibrils leading to VSMC contraction is driven by two synergistic biochemical pathways: the calcium-dependent activation of myosin light chain kinase (MLCK) and the inhibition of myosin light chain phosphatase (MLCP) through the RhoA-ROCK pathway (Ahmed and Warren 2018). Complete models of these biochemical pathways would require a high degree of parameterization to realize the full network structure and biochemistry (Chen et al. 2010), a parameterization that can be difficult, if not impossible. To overcome these limitations, logic-based models that operate on qualitative descriptions of signaling networks have been developed (Kraeutler et al. 2010; Irons and Humphrey 2020; Yoshida et al. 2022). These more general models do not require precise rate parameter definitions for each species interaction, but they are still capable of capturing tissue-scale responses to perturbed biochemical signaling.

To overcome some current limitations of in silico TFM models, we present a comprehensive structural bio-chemo-mechanical model of TFM experiments in VSMCs. The model incorporates advances from systems biology, biomedical engineering, and engineering mechanics to integrate intracellular signaling with actomyosin contraction and the resulting cytoskeletal and substrate deformation. The model operates on both a single activation pulse and cyclic signaling to recapitulate steady-state behavior. We demonstrate that the flexibility of this technique allows for the accurate prediction of experimental results under reduced RhoA signaling, varied cellular geometries, and increased substrate stiffnesses. The presented model captures the complex interplay among biological, chemical, and mechanical signaling in cellular contractile force generation, providing a tool for interpreting, and applying TFM data in the evaluation of new ideas in mechanobiology.

2 Methods: multiphysical model

A summary of the materials and methods is provided below. Additional methodological detail is included in the supplement.

The structural bio-chemo-mechanical model operates on four interacting components (Fig. 1):

- A biochemical signaling network (Fig. 1a) that takes mechanical and chemical signals as inputs and produces an actomyosin contractility signal level output.
- An actomyosin contractile element (Fig. 1b) that converts the actomyosin contractility signal level into a force/length/velocity relationship for the actomyosin fiber bundles.
- A cytoskeletal network (Fig. 1c) that determines the mechanical equilibrium between the individual fiber bundles based on their interconnections and the elastic substrate attachments.
- The underlying elastic substrate (Fig. 1d) that is attached to the simulated VSMC through focal adhesions.

2.1 Cell signaling network

The biochemical signaling network (Fig. 1a) operates on a system of ordinary differential equations (ODEs), each representing a signaling species, which are connected through logic-based relations. This approach is well documented in qualitatively mapping biochemical signaling networks to mechanical responses in both smooth and striated muscle cells (Irons and Humphrey 2020; Kraeutler et al. 2010; Yoshida et al. 2022). In VSMCs, the sliding of activated myosin heads along actin filaments generates a contractile force. Two synergistic biochemical pathways lead to myosin and actin activation: calcium-dependent activation of myosin light chain kinase (MLCK) and inhibition of myosin light chain phosphatase (MLCP) via the RhoA-ROCK pathway (Ahmed and Warren 2018). To model this activation, 21 signaling species are selected from a system formulated by Irons (Irons and Humphrey 2020). Only nodes that contribute to actomyosin activation, not long-term remodeling, are included due to the short time frame of TFM experiments, and a graphical representation of this signaling
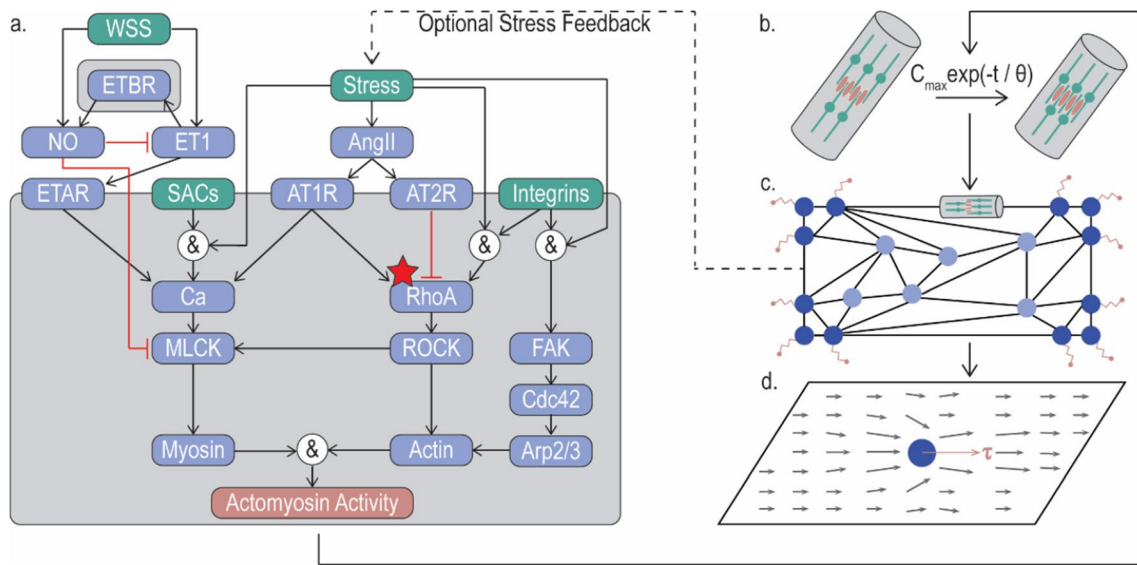
Fig. 1 Structural bio-chemo-mechanical model schematic. **a** Biochemical signaling network of VSMC intracellular signaling determines the activation signal that drives **b** actomyosin bundle contraction through the parameter C_{max}. **c** Simulated VSMCs are represented as rectangular cytoskeletal networks of free nodes (light blue) and focal adhesions (dark blue) that attach the cell to the underlying substrate. **d** Substrate displacement due to focal adhesion-applied traction stress is determined as the superposition of circular contacts applying tangential stress on an elastic half-space. Colors in signaling network represent input species (green), intermediates (blue), and output species (pink)

network describes how the nodes (signaling species) interact with one another via edges (Fig. 1a). Logic statements are used to combine the effects of the edge relationships for each node (listed in Table S1).

Following the approach of Kraeutler et al. (Kraeutler et al. 2010), a system of nonlinear ODEs is constructed from the logic statements with each node's activation described as a normalized Hill function

$$F(X) = \frac{BX^n}{(B-1) + X^n} \quad (1)$$

where the Hill coefficient n determines the steepness of the function, and the constant B enforces the constraints

$$F(0) = 0 \quad (2)$$

$$F(1) = 1 \quad (3)$$

$$F(EC_{50}) = 0.5 \quad (4)$$

The EC_{50} is defined as the value of X where half-maximal activation occurs, resulting in B being defined as

$$B = \frac{EC_{50}^n - 1}{2EC_{50}^n - 1} \quad (5)$$

The use of normalized Hill functions to model node activation converts traditional discrete Boolean descriptors into continuous formulations within the interval [0, 1]. For edges describing activating relationships (solid black arrows in Fig. 1a), Eq. (1) is used. For edges where the relationship is inhibitory (dashed red, flat-headed arrows in Fig. 1a), Eq. (1) is negated via $1 - F(X)$.

The logic-based relationships used to combine the edge relationships utilize three conditional operators, 'AND' ($\land$), 'OR' ($\lor$), and 'NOT' ($\neg$). These operators are defined mathematically according to

$$X \land Y = F(X)F(Y) \quad (6)$$

$$X \lor Y = F(X) + F(Y) - F(X)F(Y) \quad (7)$$

$$\neg X = 1 - F(X) \quad (8)$$

The transient activation of each species node (Y_i) is modeled according to the general ODE form

$$\frac{dY_i}{dt} = \frac{1}{\tau_i}\left(w_i Y_{i_{max}} G_{i_{act}} - Y_i\right) \quad (9)$$

where τ_i is the decay time, w_i is the reaction weight, $Y_{i_{max}}$ is the maximal activity level [0, 1], and $G_{i_{act}}$ is the combination of activation signals for species i. Details on the determination of biochemical network parameters and a sensitivity study are included in the supplement.

The biochemical signaling network is incorporated into the model via the open-source code "Netflux" (Kraeutler

et al. 2010). The system of ODEs is solved numerically between 0 and 100 s, well over the time for steady state to be established for any signaling species. The steady-state value of the "Actomyosin Activity" node sets the maximum stress fiber activation, C_{max}, in the fiber-level component.

2.2 Stress fiber contraction

Actomyosin stress fiber bundle contraction is determined with C_{max} as an input following Deshpande et al. (Deshpande et al. 2006), but the equations are applied to individual fiber bundles instead of continuously throughout the geometry. Stress fiber changes are the result of three interacting phenomena:

1. A biochemical activation signal triggers a remodeling response.
2. The stress fibers become more robust according to this signal or dissociate if the tension throughout the fiber bundle is too low.
3. The stress fibers contract actively, developing tension throughout, as the myosin heads engage with actin filaments.

Each stress fiber in the network is modeled discretely, but the maximum stress fiber activation, C_{max}, obtained from the biochemical signaling network is applied uniformly. The biochemical activation is modeled as an exponential decay with time constant θ from this initial maximum value. The stress fiber reinforcement and dissociation are modeled as a first-order kinetic equation

$$\frac{d\eta}{dt} = (1 - \eta)\frac{k_f}{\theta}\left[C_{max}\exp\left(\frac{-t}{\theta}\right)\right] - \left(1 - \frac{\sigma}{\sigma_0}\right)\frac{k_b}{\theta}\eta \qquad (10)$$

where η is the fiber activation, t is simulation time, k_f and k_b are rate parameters describing the formation and dissociation of fiber components, and σ/σ_0 is the normalized fiber stress. The normalized active fiber stress, σ/σ_0, is described with a logistic function:

$$\frac{\sigma}{\sigma_0} = \left(1 + \exp\left(-5.301\left(\frac{\dot{\lambda}}{\dot{\lambda}_0} + \frac{\eta}{2k_v}\right)\right)\right)^{-1} \qquad (11)$$

where the parameter k_v governs the reduction in fiber stress according to the contraction strain rate $\dot{\lambda}$. This logistic function was found by fitting a continuous function to the original piecewise formulation (Deshpande, McMeeking, and Evans 2006). The active fiber stress is normalized according to the isometric stress, σ_0, which is defined as the product of the activation level and the maximum tensile stress allowed by biochemistry, σ_{max}. The passive fiber stress due to fiber strain, λ, is given by:

$$\sigma_p = \frac{E}{B}\left(\exp\left(\frac{B(\lambda^2 - 1)}{2}\right) - 1\right) \qquad (12)$$

where material constants E and B control fiber stiffness and nonlinearity, respectively. The total stress in each actomyosin fiber is the sum of the passive stress (Eq. 12) and active stress (non-normalized form of Eq. 11). Additional discussion and justification of parameter selection is included in the supplement (Section S1.2).

2.3 Cytoskeletal network

The VSMC cytoskeleton was simulated as a Delaunay network of 50 randomly seeded nodes within a $32\,\mu m \times 127\,\mu m$ region and 7 uniformly spaced nodes in each corner of the rectangular cell. The corner nodes are spaced 1 μm apart. Nodes within the interior of the cell are not attached to the underlying substrate, and the corner nodes are designated as focal adhesions. The focal adhesions attach the simulated cell to the elastic substrate and resist the stress fiber-driven network contraction.

The position of each cytoskeletal node is determined such that mechanical equilibrium is maintained. For non-focal-adhesion nodes, mechanical equilibrium requires that the sum of all forces from attached stress fibers be zero. If the cytoskeletal node is designated as a focal adhesion, an additional force associated with the substrate's resistance to displacement is incorporated. Because the substrate is modeled as linear elastic, the resistance to focal adhesion displacement acts as a linear spring. A symmetric matrix of spring constants is constructed by applying a unit force in the x- and y-direction on each focal adhesion and then determining the displacement of the other focal adhesions. These displacements are then converted back into local Hookean spring constants.

The equilibrium positions of each cytoskeletal node throughout the network are found via Newton–Raphson iteration, using a numerical Jacobian matrix and an error tolerance of 10^{-8} nN. The system is assumed to be initially stress-free, and all fibers have an activation level of 0. The initial guess for subsequent time steps is set to the solution from the previous time step.

2.4 Substrate displacement

The substrate displacement field for the simulated VSMCs is found following Menga et al. (Menga and Carbone 2019). For each focal adhesion, the net force on the network node is converted to a traction t^{tot} by dividing by the assumed focal adhesion area. The angle between the traction force and the global x-axis is then calculated.

$$\theta_{FA} = \tan^{-1}\left(\frac{t_y^{\text{tot}}}{t_x^{\text{tot}}}\right) \tag{13}$$

Each focal adhesion traction contribution is rotated into a local coordinate system using a rotation matrix,

$$\begin{bmatrix} \tau \\ 0 \end{bmatrix} = \begin{bmatrix} \cos\theta_{FA} & \sin\theta_{FA} \\ -\sin\theta_{FA} & \cos\theta_{FA} \end{bmatrix} \begin{bmatrix} t_x^{\text{tot}} \\ t_y^{\text{tot}} \end{bmatrix} \tag{14}$$

such that the local applied traction, τ, is only in the 1-direction. This local stress is then translated into a displacement field, in the local coordinate system, using Menga's expressions (Menga and Carbone 2019):

$$\tilde{u}_1 = \begin{cases} \frac{\tau a}{\pi G}\left[(2-\nu)E(\rho) + \frac{\nu\cos 2\theta}{3\rho^2}\left((2-\rho^2)E(\rho) - 2(1-\rho^2)K(\rho)\right)\right] & \rho < 1 \\ \frac{\tau a}{\pi G}\left[2(1-\nu)\rho\left(E\left(\frac{1}{\rho}\right) - \left(1-\frac{1}{\rho^2}\right)K\left(\frac{1}{\rho}\right)\right) + \nu E(\varphi,\rho) + \frac{\nu\cos 2\theta}{3\rho^2}\left((2-\rho^2)E(\varphi,\rho) - 2(1-\rho^2)F(\varphi,\rho)\right)\right]_{\varphi=\varphi_2-\theta-\pi} & \rho > 1 \end{cases} \tag{15}$$

$$\tilde{u}_2 = \begin{cases} \frac{\nu\tau a\sin 2\theta}{3\pi G\rho^2}\left[(2-\rho^2)E(\rho) - 2(1-\rho^2)K(\rho)\right] & \rho < 1 \\ \frac{\nu\tau a\sin 2\theta}{3\pi G\rho^2}\left[(2-\rho^2)E(\varphi,\rho) + 2(1-\rho^2)F(\varphi,\rho)\right]_{\varphi=\varphi_2-\theta-\pi} & \rho > 1 \end{cases} \tag{16}$$

where r and θ are the polar coordinates describing the point in space in the local focal adhesion coordinate system, $\rho = r/a$, a is the focal adhesion radius, and ν and G describe the elastic properties of the substrate. The complete and incomplete elliptic integrals of the first and second kind ($E(\rho)$, $E(\varphi,\rho)$, $K(\rho)$, and $F(\varphi,\rho)$) are calculated in MATLAB. The complete displacement field due to the simulated cell traction is constructed through superposition of the displacement fields following rotation back into the global coordinate system.

The following default parameters describing the elastic substrate were used unless noted. The focal adhesion radius, a, is set to $\sqrt{3/\pi}\mu$ m (Hou et al. 2019). The substrate stiffness, G, is set to 12 kPa, and Poisson's ratio, ν, is set to 0.48.

2.5 Single-stimulus vs. feedback mode

The structural bio-chemo-mechanical model operates both with a single activation signal (following Deshpande et al. (Deshpande, McMeeking, and Evans 2006)) and with feedback (describing the more common situation in which a steady traction is developed). When feedback is incorporated, the average actomyosin bundle stress within the cytoskeleton (Fig. 1c) is normalized and returned to the biochemical signaling network (Fig. 1a) as the "Stress" input. The newly established steady-state value for "Actomyosin Activity" determines a new C_{max} after a transition period

of 60 s during which the cell equilibrates its biochemical signaling.

3 Methods: comparison with experimental results

The modeling scheme was applied to three separate test cases–affecting three different aspects of the model–based on experiments published previously by others. Specifically, a SUN1 knockdown (Porter et al. 2020) changed the biochemical signaling of the system, cell aspect ratio control (Win et al. 2017) changed the cytoskeletal network, and experiments with different substrate stiffnesses (Huynh et al. 2013) changed the mechanical interaction between the cell and the substrate. These three cases are further described below.

3.1 Case 1: SUN1 knockdown

The incorporation of biochemical signaling into the structural bio-chemo-mechanical model allows for the comparison of the simulated results to TFM experiments on VSMCs. Porter et al. (Porter et al. 2020) investigated the role of SUN1, a key component of nuclear membrane LINC complexes, in conferring extracellular mechanical signals to the VSMC nucleus. When SUN1 was knocked down, Porter (Porter et al. 2020) observed a reduction in the activity of RhoA, which plays an integral role in coordinating VSMC contraction through the ROCK pathway. While Porter (Porter et al. 2020) demonstrated that a reduction in SUN1 signaling led to a downstream decrease in RhoA activity, they did not present a clear mechanism connecting the two signaling species, so to recapitulate the experimental changes in signaling due to SUN1 knockdown, the maximum activity of the "RhoA" node within the biochemical cell signaling network was reduced from 1 to 0.3.

The simulated traction stresses were scaled such that the control results were at a comparable magnitude to the values reported by Porter et al. (Porter et al. 2020). To achieve proper scaling, the maximum active fiber stress, σ_{max}, was set to 0.7 kPa, matching the cell stress at steady state to the experimental value.

3.2 Case 2: altered cell geometry

It is not uncommon for groups to micropattern VSMCs in conjunction with biochemical treatments, such as nocodazole or cytochalasin D (Win et al. 2017), but we elected to demonstrate the power of our model by isolating each component's ability to capture experimental trends independently. Win et al. (Win et al. 2017) demonstrated that VSMCs micropatterned into elongated geometries not only respond differently to dynamic loading conditions but also exhibit increasingly anisotropic fiber distributions. As the micropattern aspect ratio increases, the preferential alignment of stress fibers in the direction of elongation also increases (Win et al. 2017). When cytoskeletal nodes in the model are randomly seeded in the elongated geometries, there is a degree of natural anisotropy within the fiber distribution, but it does not match the level seen experimentally (described further under results). VSMCs were also simulated (details in supplemental methods) with prescribed fiber orientations close to the experimental fiber angle distributions. To underscore the effects of cytoskeletal geometry, feedback mode was used.

The model results were scaled to match the traction stresses reported by Win et al. (Win et al. 2017). The parameter σ_{max} was set to 0.397 kPa in the stress feedback setting. The new σ_{max} value was chosen such that the simulated traction stresses at steady-state in the 1:1 aspect ratio with prescribed fiber alignment cases matched the respective results by Win et al. (Win et al. 2017).

3.3 Case 3: substrate stiffness variations

In their analysis of circular dorsal ruffle formation, Huynh et al. (Huynh et al. 2013) reported that VSMCs generate more contractile force on stiff substrates. The simulated substrate stiffnesses were modeled by altering the shear modulus, G (Eqs. 15, 16), to match those reported by Huynh et al. (Huynh et al. 2013). For the altered focal adhesion (FA) cases, the original networks were altered to include more FAs in each corner (Table S4). The number of FAs were scaled linearly with substrate stiffness. An additional focal adhesion in each corner was incorporated in some cases to maintain symmetry throughout the corner with a single FA in the corner apex. The spacing between each FA was kept consistent at 1 μm, and the total number of interior nodes was also consistent at 50. For the non-altered FA cases, the number of FAs and interior nodes was 28 and 50, respectively. The simulated traction forces were scaled to match the experimental data by setting σ_{max} to be 0.35 kPa in the constant FA cases and 2.85 kPa in the scaled FA cases. The new σ_{max} values were chosen such that the steady-state traction force in the 2.5 kPa substrate comparisons matched the respective traction forces reported by Huynh

et al. (Huynh et al. 2013). The increased order of magnitude in σ_{max} for the scaled FA cases is the result of fewer focal adhesions in the initial 2.5 kPa substrate simulations (only 4 total) needing to achieve the same traction force as the non-scaled case (28 total).

Huynh et al. (Huynh et al. 2013) also reported that treatment with ML-7, a MLCK inhibitor, counteracted the increased contractility observed on stiff substrates. The ML-7 treatment was modeled by reducing the maximum activity of the "MLCK" node from 1 to 0.2 in the biochemical signaling network. The focal adhesions were scaled with increasing substrate stiffness. All other model considerations were kept consistent with the substrate stiffness comparisons done under control conditions.

3.4 Statistical analysis

Model results were considered to match published experimental data if the mean of the simulated traction stresses fell within the experimental 95% confidence interval. Further numerical determination of statistical significance was deemed inappropriate since the in silico and in vitro results have vastly different sources and sizes of error.

3.5 Implementation

The structural bio-chemo-mechanical model is implemented in MATLAB.

4 Results

4.1 General model behavior

Beginning with single-stimulus mode, when a single activation signal was applied and allowed to decay exponentially with time constant θ (Fig. 2a–c), actomyosin stress and traction force rose in response to the signal and then decayed as the activation was lost. The application of a single activation pulse mimics the conditions used in previous theoretical work (Deshpande, McMeeking, and Evans 2006), but the decay of traction force is not typically observed in in vitro TFM experiments. At t/θ = 1.5, there is large substrate displacement near the focal adhesions that dissipates quickly toward the VSMC interior (Fig. 2d). Additionally, fiber activity is maximized uniformly throughout the cytoskeletal network. The substrate displacement and fiber activities follow the decay of the activation signal, approaching zero after t/θ = 10 (Fig. 2e–f). The activation signal from the biochemical signaling network (Fig. 1) is applied uniformly
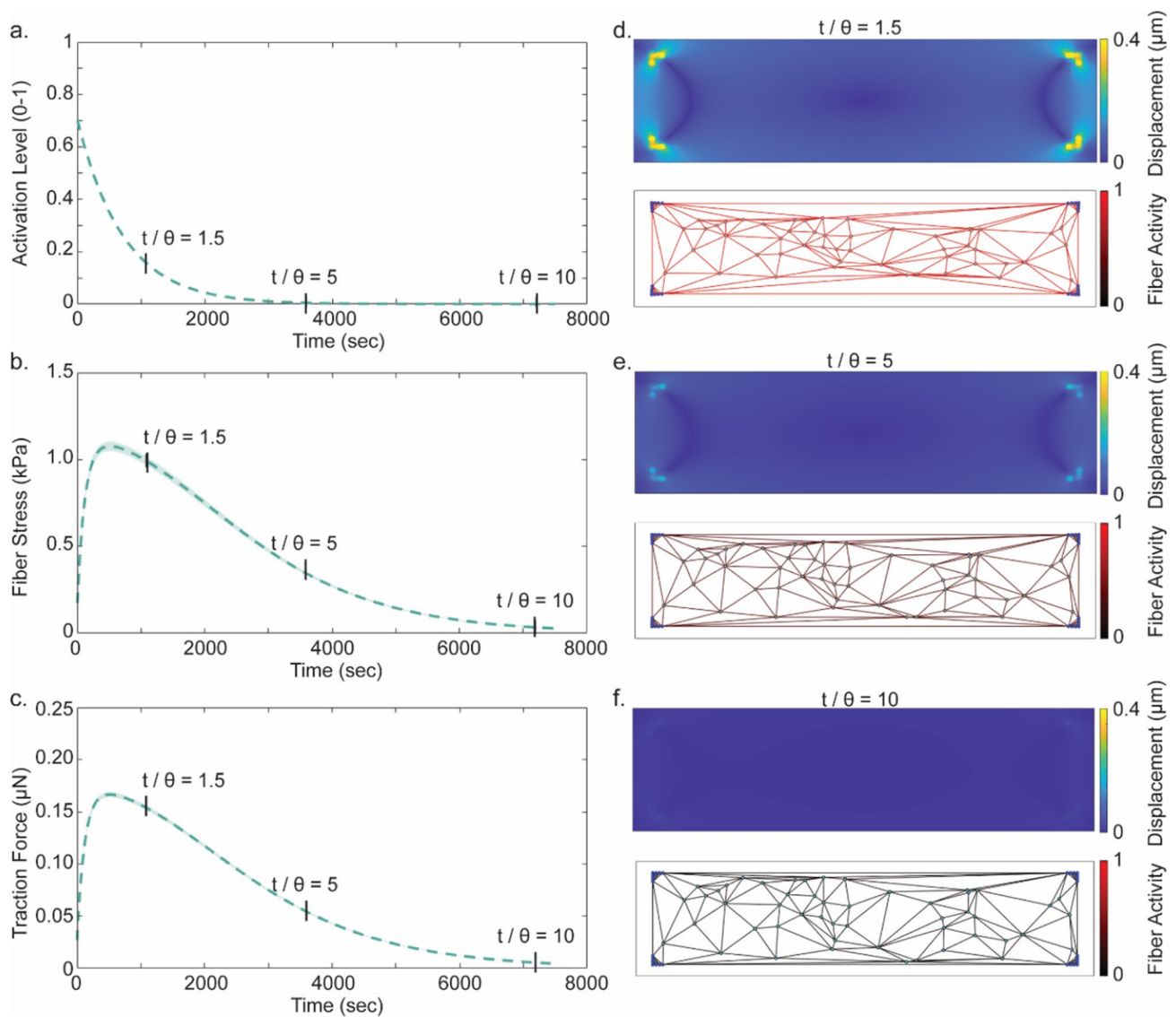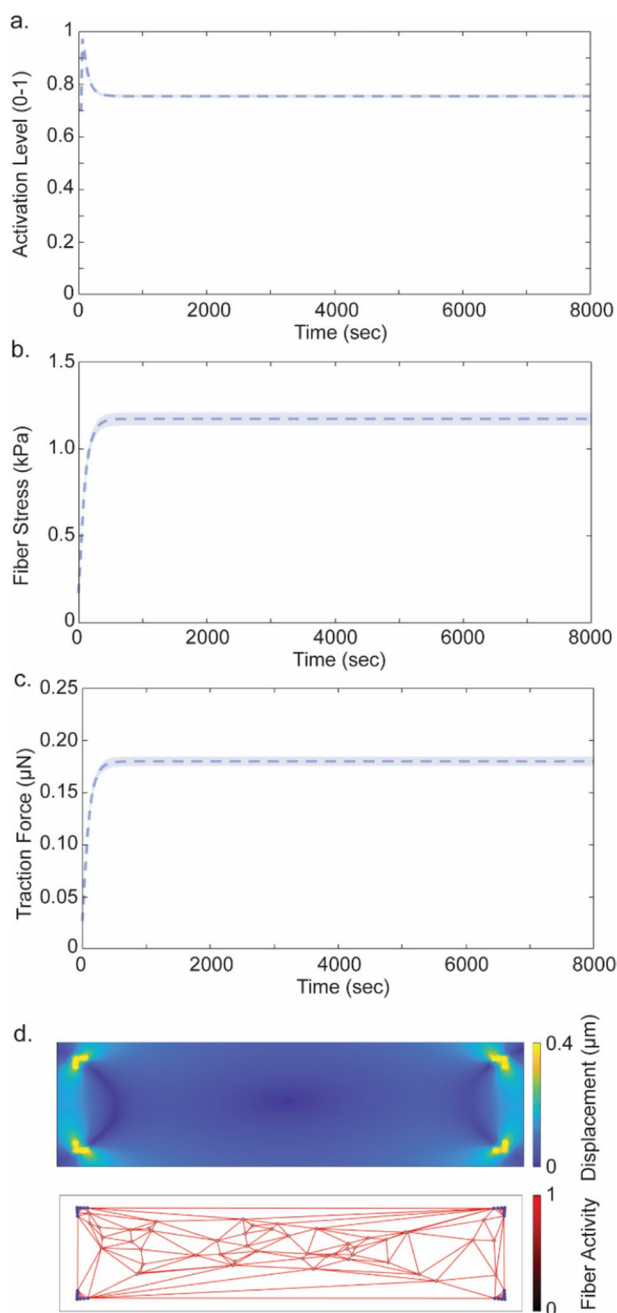
Fig. 2 a Activation signal decay, **b** actomyosin bundle stress, and **c** focal adhesion traction force after a single pulse under baseline conditions. Representative substrate displacement fields (top) and cytoskel-etal network fiber activations (bottom) at d. $t/\theta = 1.5$, e. $t/\theta = 5$, and f. $t/\theta = 10$. Shaded regions in (a.-c.) are the 95% confidence interval for $n = 5$

throughout the cytoskeleton, and thus, the activation of individual fiber bundles (Fig. 2d–f) is approximately uniform.

To better capture the contractility observed in TFM, we implemented a feedback loop in which the mean fiber stress was normalized and then input into the biochemical signaling network, generating a new activation signal. In this stress feedback condition, the activation signal, mean fiber stress, and applied traction forces all approached steady-state behavior (Fig. 3a–c). The implementation of stress feedback, however, did not change the localization of substrate displacement near focal adhesions, nor did it change the uniform distribution of stress fiber activation throughout

the cytoskeleton (Fig. 3d). There is not a large difference between the maximum traction stress applied in the single pulse setting and the steady-state traction stress in the feedback setting, making the two modes largely interchangeable if one's objective is to compare two responses. Since the implementation of stress feedback more closely matches the conditions observed in traditional TFM, however, the following experimental comparisons were all completed with feedback incorporated.

Fig. 3 a Activation signal, **b** actomyosin bundle stress, and **c** focal adhesion traction force with stress feedback applied under baseline conditions. **d** Representative substrate displacement field (top) and cytoskeletal network fiber activations (bottom) at steady state. Shaded regions in (**a–c**) are the 95% confidence interval for $n=5$

4.2 SUN1 knockdown

The reduction in RhoA activity (Fig. 4a) resulted in a 75% decrease in the initial activation signal pulse from the cell signaling network (Fig. 4b). The mean actomyosin bundle stress and focal adhesion-applied force also decreased in

the simulated SUN1 knockdown VSMCs (Fig. 4c–d). The approach toward steady state with the inclusion of stress feedback is similar between the two cases. The simulated VSMC data generated by the structural bio-chemo-mechanical model recapitulated the experimental results generated by Porter et al. (Porter et al. 2020). When the mean actomyosin bundle stress at steady state is normalized to that of the siControl case, both the in silico and in vitro VSMCs have a 40% decrease in stress (Fig. 4e). Additionally, when compared to the control VSMCs (Fig. 4f), the simulated SUN1 knockdown VSMCs generate less substrate displacement through the focal adhesions (Fig. 4g). The decrease in contractile behavior is driven by the reduced activation of the actomyosin stress fiber bundles (Fig. 4f–g bottom), and thus less active stress is transferred through the focal adhesions to the elastic substrate.

4.3 Altered cell geometry

The structural bio-chemo-mechanical model also captures the effect of cell geometry and actomyosin fiber alignment throughout the cytoskeleton. The activation signal, fiber bundle activation and stress, and focal adhesion-applied traction force reach steady-state by approximately 1000 simulated seconds due to the recursive signaling from the cytoskeletal stress back into the biochemical signaling network (Figure S1). The networks without prescribed alignment become slightly more aligned during equilibration, but do not approach the experimental degree of alignment (Figure S2).

Win et al. (Win et al. 2017) demonstrated that VSMCs micropatterned in elongated geometries exhibited higher traction forces and increasingly anisotropic stress fiber distributions. While the random seeding of interior nodes resulted in some anisotropy (Fig. 5a, c, e, g), the interior nodes needed to be preferentially seeded to achieve the experimentally reported degrees of anisotropy in elongated geometries (Fig. 5b, d, f, h). When the maximum tensile stress, σ_{max}, was scaled such that the 1:1 aspect ratio simulations match the respective experimental data at steady state, the simulated traction stresses fall within the experimental error both when the stress fibers are prescribed an alignment and when they are not (Fig. 6). The simulated traction stresses when the networks were aligned according to experimental data, however, more closely followed the trend of increased stress generation in elongated VSMCs. The in silico results from VSMCs without pre-aligned actomyosin stress fibers did not exhibit increased normalized traction stress; however, the results did not fall out of the reported experimental error range. VSMCs micropatterned into a 1:1 aspect ratio exhibited isotropic fiber distributions, and therefore no difference was observed between the prescribed
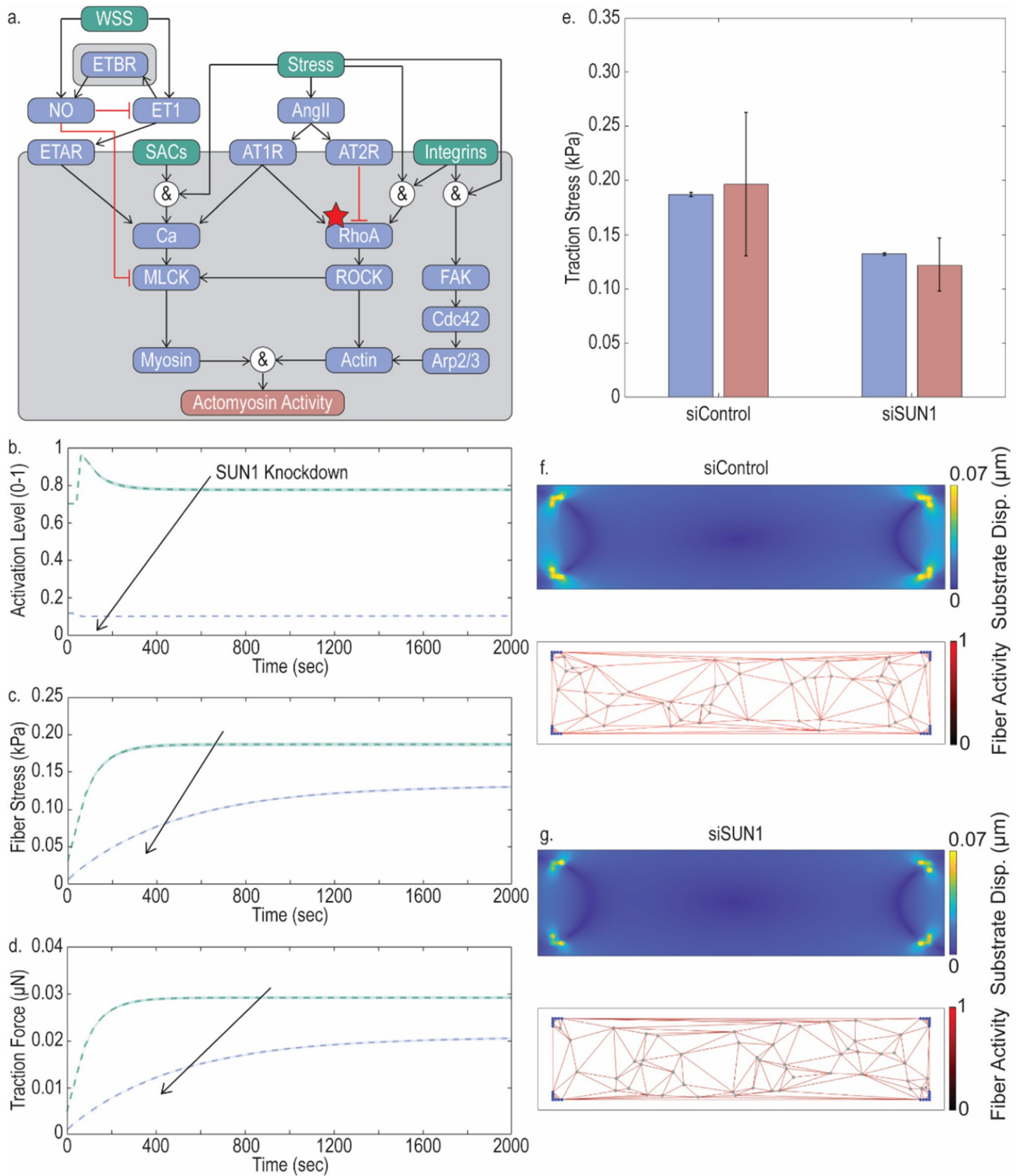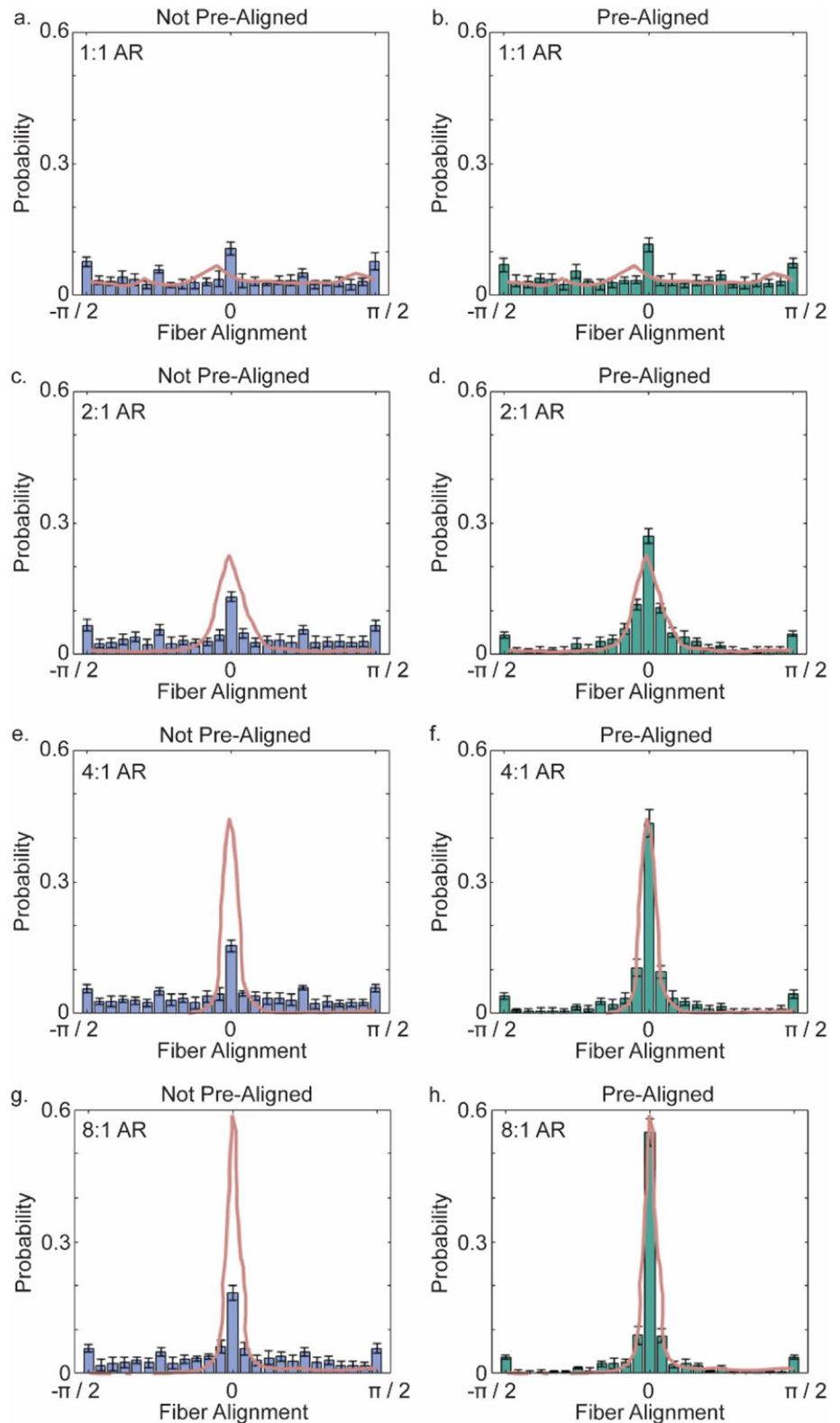
Fig. 4 Structural bio-chemo-mechanical model is consistent with experimental data with altered biochemical signaling. **a** siSUN1 knockdown is represented by a reduction in RhoA (starred) activity within the biochemical signaling network. **b** A activation signal, **c** mean actomyosin bundle stress, and **d** total traction force under control and reduced RhoA activity. Arrows point from siControl to siSUN1 knockdown cases. **e** Mean traction stress at steady-state (blue) compared to experimental data (pink) generated by Porter et al. The maximum tensile stress, σ_{max}, is scaled such that the peak tensile stress matches the experimentally reported value for the siControl case. **f.-g.** Representative substrate displacement fields (top) and cytoskeletal networks (bottom) at steady state for the simulated control and reduced RhoA VSMCs. Shaded regions in **b–d** and error bars in **e.** are SEM for $n = 15$

and non-prescribed simulations (Fig. 7a). In the elongated geometries, for which highly anisotropic distributions were observed, there was a difference in simulated contractile response. In 2:1 and 4:1 aspect ratios, the VSMCs with

prescribed fiber alignments exhibited increased contractility in the direction of alignment, which translated to increased displacement of focal adhesions toward the interior of the cell (Fig. 7b, c). The translation of focal adhesions toward
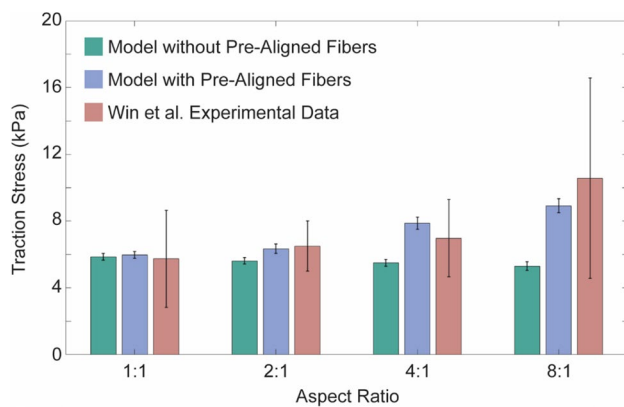
Fig. 6 Structural bio-chemo-mechanical model recapitulates experimentally observed changes in traction stress in elongated geometries with highly aligned cytoskeletal networks. Traction stress at steady state in in silico VSMCs with and without prescribed alignment compared to in vitro TFM data. The maximum tensile stress, σ_{max}, is scaled such that the steady-state tensile stress matches the experimentally reported value for 1:1 AR case. Error bars are standard deviation for $n = 10$

the centerline of the cell was also observed in the 8:1 aspect ratio, but this behavior was also accompanied with a visible increase in substrate displacement on the narrow ends of the simulated cell (Fig. 7d).

4.4 Substrate Stiffness Variations

A third manipulable component of the structural bio-chemo-mechanical model is the stiffness of the underlying elastic substrate. To underscore the mechanosensitivity of focal adhesions, feedback signaling from the cytoskeleton to the biochemical signaling network was applied, and steady state was established. The biochemical activation signal, C_{max}, achieved steady state after approximately 800 s of simulated time, with similar dynamics across the various stiffnesses (Fig. 8a). The set designations of nodes as focal adhesions or not failed to account for the well-established response of cells to increase the size and number of focal adhesions on stiff substrates (Yeh et al. 2017). When the number of focal adhesion attachments was scaled according to substrate stiffness, the rate at which steady state was approached remained constant with increasing stiffness; however, there was more variation in the value approached (Fig. 8b). The biochemical activation signal was decreased in systems with stiffer substrates, and this separation was amplified by the greater number of focal adhesions. The mean actomyosin bundle stress was increased in stiffer systems, however (Fig. 8c). The fiber stress was greatly decreased in the soft 2.5 kPa substrate cases when the focal adhesions were decreased (Fig. 8d). The force exerted by focal adhesions followed the trend observed in actomyosin bundle stress where stiffer

substrates led to increased traction stress (Fig. 8e). Additionally, there was no observable difference in the rate of approach toward steady state with scaled focal adhesions (Fig. 8f). Throughout the simulation behavior, the stiffer systems produced increased contractile behavior with the trends more pronounced in the scaled focal adhesion cases. The paradoxical relationship between a decrease in activation signal (Fig. 8a, b) and increase in fiber and traction stresses (Fig. 8c, d, e, f) is a result of passive stress differences across the various substrates. The softer substrates allow for more stress fiber shortening, leading to greater (more negative) passive stresses (Figure S3). The total stress, therefore, is smaller in these cases.

In investigations of circular dorsal ruffle formation, Huynh et al. (Huynh et al. 2013) demonstrated that VSMCs generated increased traction force on stiffer substrates. Following scaling to match the 2.5 kPa cases, our model produced simulated VSMC traction force that also increased with increasing substrate stiffness, falling within the experimental error at intermediate stiffnesses (Fig. 9). However, at high stiffnesses, the model results are not within the error interval. In its base formulation, our model did not account for the well-established feedback between stiffness and focal adhesion development (Yeh et al. 2017). In stiffer environments, VSMCs form more and larger focal adhesions, so to mimic this relationship, we scaled the number of focal adhesions with the stiffness of the substrate. With this scaling, the simulated traction forces fell within the experimental error interval at each stiffness and more closely matched the observed increase in contractility (Fig. 9).

As expected, there was greater substrate displacement on softer substrates than stiffer ones (Fig. 10). While simulated VSMCs generated increased traction forces on stiffer substrates, the increased forces were not enough to overcome the increased resistance of the substrate to displacement. This result was consistent with a 30-fold increase in substrate stiffness inducing only a 3.5-fold increase in traction stress. The substrate displacement contribution from each focal adhesion was not consistent between the scaled (Fig. 10b, d, f, h) and non-scaled (Fig. 10a, c, e, g) cases despite differences in fiber bundle stress throughout the network; however, this results from the order of magnitude difference in scaling factors. A larger maximum fiber stress is required in the scaled FA cases since the initial 2.5 kPa cases have only 4 total FAs compared to the non-scaled, 2.5 kPa cases having 28.

4.5 Coupled biochemical and mechanical changes

The power of the structural bio-chemo-mechanical model is in the inclusion of interacting components that capture the multiple signaling processes that drive cell contractility. In
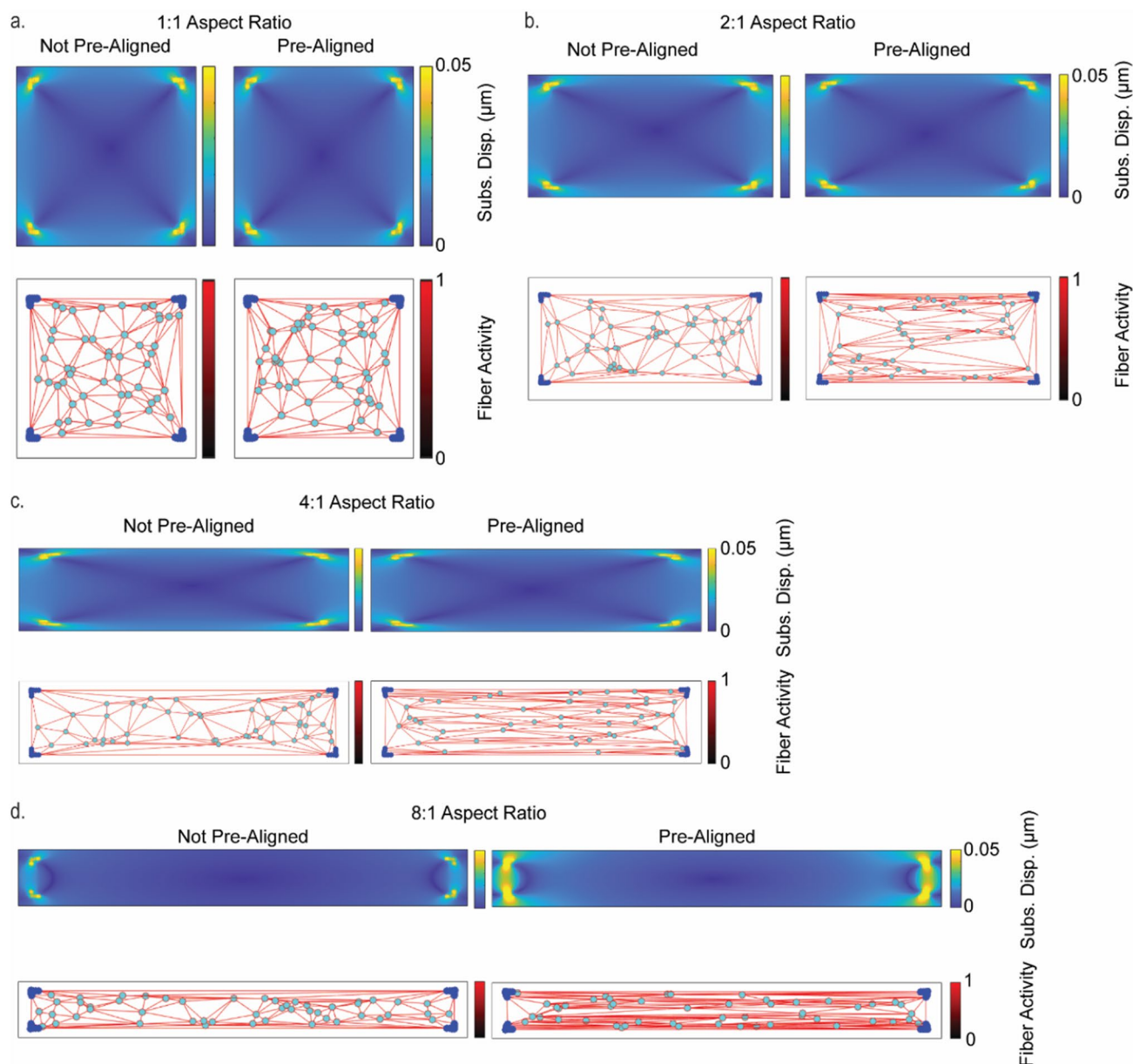
Fig. 7 Simulated substrate displacement is more pronounced in elongated VSMCs. Representative substrate displacement fields (top) and cytoskeletal networks (bottom) for simulated VSMCs with **a**. 1:1, **b**. 2:1, **c**. 4:1, and **d**. 8:1 ARs

Huynh et al.'s investigation of circular dorsal ruffle formation, the substrate stiffness-dependent contractility changes were coupled with the effects of a MLCK inhibitor, ML-7 (Huynh et al. 2013). Using the parameters and focal adhesion scaling implemented in the stiffness comparisons, the effect of MLCK inhibition was probed with the reduction of in silico MLCK activity. The implementation of MLCK inhibition reduced both the simulated and experimental VSMC traction forces (Fig. 11). The combined stiffness and MLCK inhibition model results follow the trend at each stiffness; however, the model slightly underestimates the traction force

on 5 kPa and 10 kPa substrates and slightly overestimates the traction force on the 30 kPa substrate.

5 Discussion

Traction force microscopy (TFM) is a widely used experimental technique in mechanobiology, allowing the interactions between cell and substrate to be probed to reveal in vitro contractility. The ease and flexibility of TFM has led to its application to many contractile cell types, including vascular smooth muscle cells (VSMCs). The results of

Fig. 8 Stiffness-dependent differences in simulated VSMC behavior are exacerbated by focal adhesion scaling. **a** Activation signal, **c** actomyosin bundle stress, and **e** focal adhesion force evolution with cyclic signaling and focal adhesions constant across substrate stiffnesses. **b** Activation signal, **d** actomyosin bundle stress, and **f** focal adhesion force evolution with cyclic signaling and increasing focal adhesion numbers with increasing substrate stiffness. Arrows in **a**.–**f**. point in the direction of increasing substrate stiffness for the four assayed values (2.5, 5, 10, and 30 kPa). Shaded regions are SEM for $n = 12$
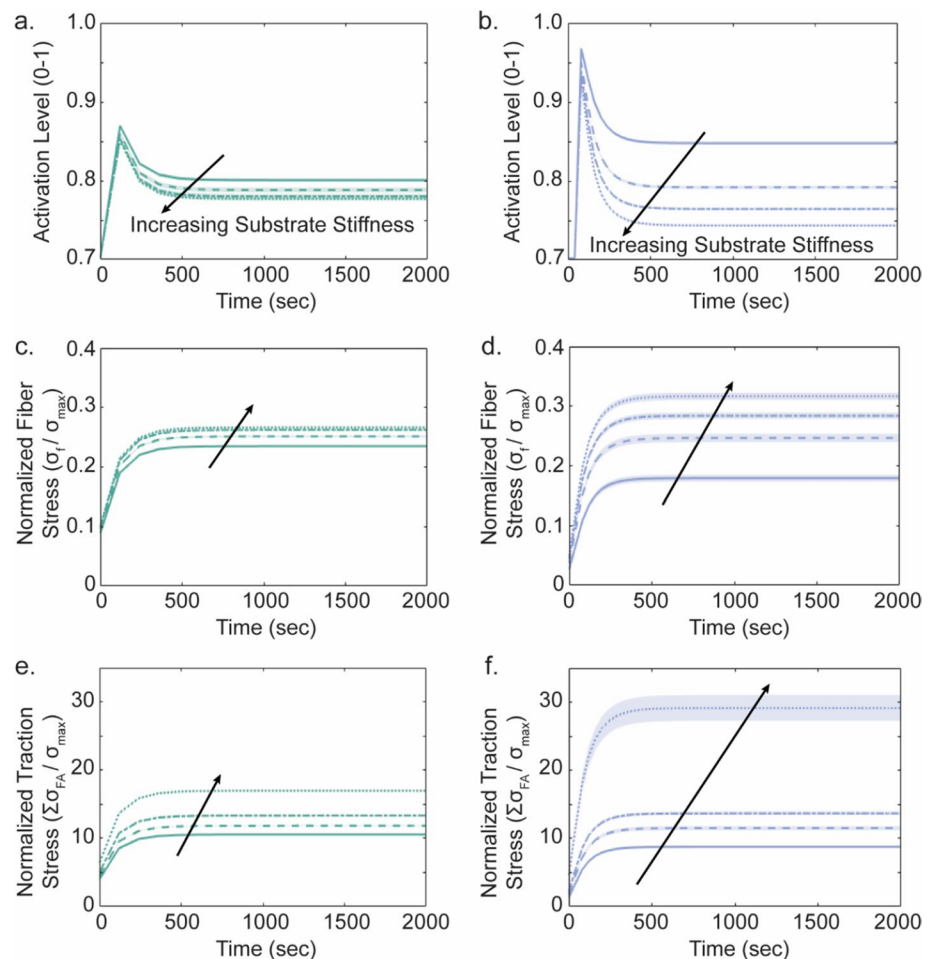

TFM experiments have led to several discoveries about how cells respond to their mechanical environment, such as increasing focal adhesion contact area to increase traction force (Balaban et al. 2001; Goffin et al. 2006; Yeh et al. 2017), altering spreading and migration due to changes in substrate stiffness (Trichet et al. 2012), stiffness-sensitive guidance during stem cell differentiation (Wen et al. 2014), and mechanical changes in response to chemical cues (Porter et al. 2020). The wealth of available experimental data, coupled with the ease with which more can be produced, makes TFM a valuable resource to characterize and describe cell contractility. Despite its limitations of being a 2D in vitro assessment, the observed behavioral trends in this simplified environment are often consistent with 3D in vivo contractility. While the reported numerical values of traction stresses may not translate from the dish into the body, how the traction stresses change relative to one another when treatments are applied or geometries/substrates changed is still relevant. Computational models are in the unique position to translate the wealth of information collected in vitro into vital tissue and organism-level predictions. There is, however, a severe lack in accurate models that

encompass the multiple facets of TFM to bridge the gap between the in vitro and in vivo situations.

Models of TFM in simple geometries have been developed, but again they do not incorporate several of the processes seen in vitro. The work of Deshpande et al. (Deshpande et al. 2006) captures the spatiotemporal activation and contraction of actomyosin throughout a square VSMC, but there is minimal consideration of VSMC biochemical signaling, treating the cell as a black box that outputs a given activation signal. Additionally, the VSMC is modeled continuously with no explicit inclusion of discrete actomyosin stress fibers. The temporal contractile signal utilized by Deshpande (Deshpande et al. 2006) is also not representative of TFM experiments where the cellular behavior is at a steady state. The transient contraction captured via a single activation pulse in the model, however, does mimic the pulse-response observed in skeletal muscle fibers following an electrical pulse (Rausch et al. 2020).

The model we present incorporates four interacting components to capture experimental trends and has the potential to serve as a conduit between future models of VSMC contractility and experimental TFM data. The
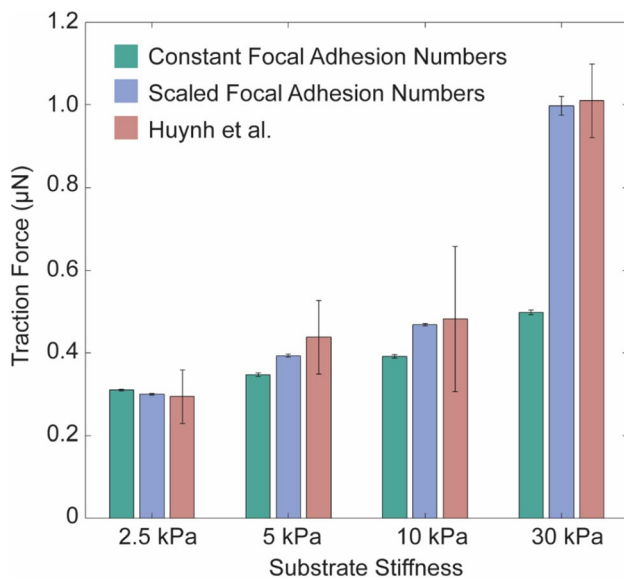
Fig. 9 Structural bio-chemo-mechanical model captures VSMC traction stress changes with increasing substrate stiffness. Steady-state traction force for constant and scaling FA numbers in silico predictions and in vitro Huynh et al. experimental data. The maximum tensile stress, σ_{max}, is scaled such that the in silico 2.5 kPa traction forces match the reported experimental value. Error bars are SEM for $n = 12$

biochemical network includes key signaling species that lead to the engagement of myosin heads onto actin filaments (Irons and Humphrey 2020). Through its inclusion, the biochemical signaling network allows the model to predict the contractile behavior of VSMCs derived from disease models or pharmacologically treated samples where biochemical pathways have been perturbed. The VSMC cytoskeletal architecture observed in vitro can also be simulated with the structural bio-chemo-mechanical model, which translates the advances of Desphande et al. (Deshpande et al. 2006) into the context of a discrete fiber network. The importance of the incorporation of discrete stress fiber networks, and their accompanying anisotropy, is demonstrated in the differential force generation between simulations with and without prescribed alignment (Win et al. 2017). Finally, the direct inclusion of substrate deformation brings VSMC stiffness mechanosensitivity into consideration (Menga and Carbone 2019). Translation across substrate stiffnesses allows for interpretation and comparison of experimental results from a variety of research groups despite the lack of a standard substrate stiffness for VSMC TFM. While the model presented herein has limitations, it offers a significant step forward in analysis and prediction of VSMC-generated forces.

The biochemical signaling network utilized in the model is constructed following state-of-the-art techniques for predicting arterial mechanobiological signaling (Irons and

Humphrey 2020). The network operates on relationships between signaling species with ordinary differential equations following a set structure. The technique, originally developed by Kraeutler et al. (Kraeutler et al. 2010) has been successfully incorporated into predictive models of arterial matrix remodeling under pressure overload (Irons et al. 2021), phenotypic manipulations with perturbed mTOR signaling observed in aortopathies (Estrada et al. 2021), heart growth during pregnancy (Yoshida et al. 2022), and biochemical signaling during heart failure (Kraeutler et al. 2010). While the signaling component model draws heavily on the biochemical modeling work completed by Irons et al. (Irons and Humphrey 2020), the incorporation of a biochemical signaling network into a multiphysical model has not been done previously. By including a component dedicated to the biochemical aspect of contractility, the effects of perturbations, such as knockdowns, of various signaling species can be modeled directly, rather than attempting to translate the effects into mechanical parameter changes (Figs. 3 and 11). In particular, the connection of biochemical signaling with a discrete cytoskeletal network allows for the investigation of how biochemical signaling and stress fiber anisotropy interact to affect VSMC contractility (Fig. 6). Additionally, translation of biochemical signaling into a meaningful traction force and stress output, rather than a normalized (0–1) activity signal as in (Irons and Humphrey 2020), is vital for the generation of a model output that is easily translatable across length scales.

An important consideration with this biochemical modeling process is that the relationships between signaling species and the resulting model outputs are qualitative and not necessarily quantitatively determined. Thus, experimental measurements of activity, such as RT-qPCR and western blotting, may not directly translate to the normalized values used in the simulated network. For example, Porter et al. (Porter et al. 2020) observed a 30% decrease in RhoA activity in their SUN1/2 knockdowns, but our model of the system (Fig. 3) recapitulated the data best with a 70% decrease in the maximum activity of the model's RhoA node. The increased inhibition of RhoA needed computationally could be the result of the parameters governing each signaling node matched qualitatively, but not necessarily quantitatively, to experimental data (Irons and Humphrey 2020). Additionally, the simplification of the biochemical signaling network results in the model results falling slightly outside the experimental range of error when other perturbations are applied, such as substrate stiffness alterations (Fig. 11). To match the in silico and in vitro biochemical relationships quantitatively, one would require several binding and reaction rate parameters for each node relationship. Even in simple networks like the one applied here, there are over 30 internodal connections, making the determination of specific parameters for each
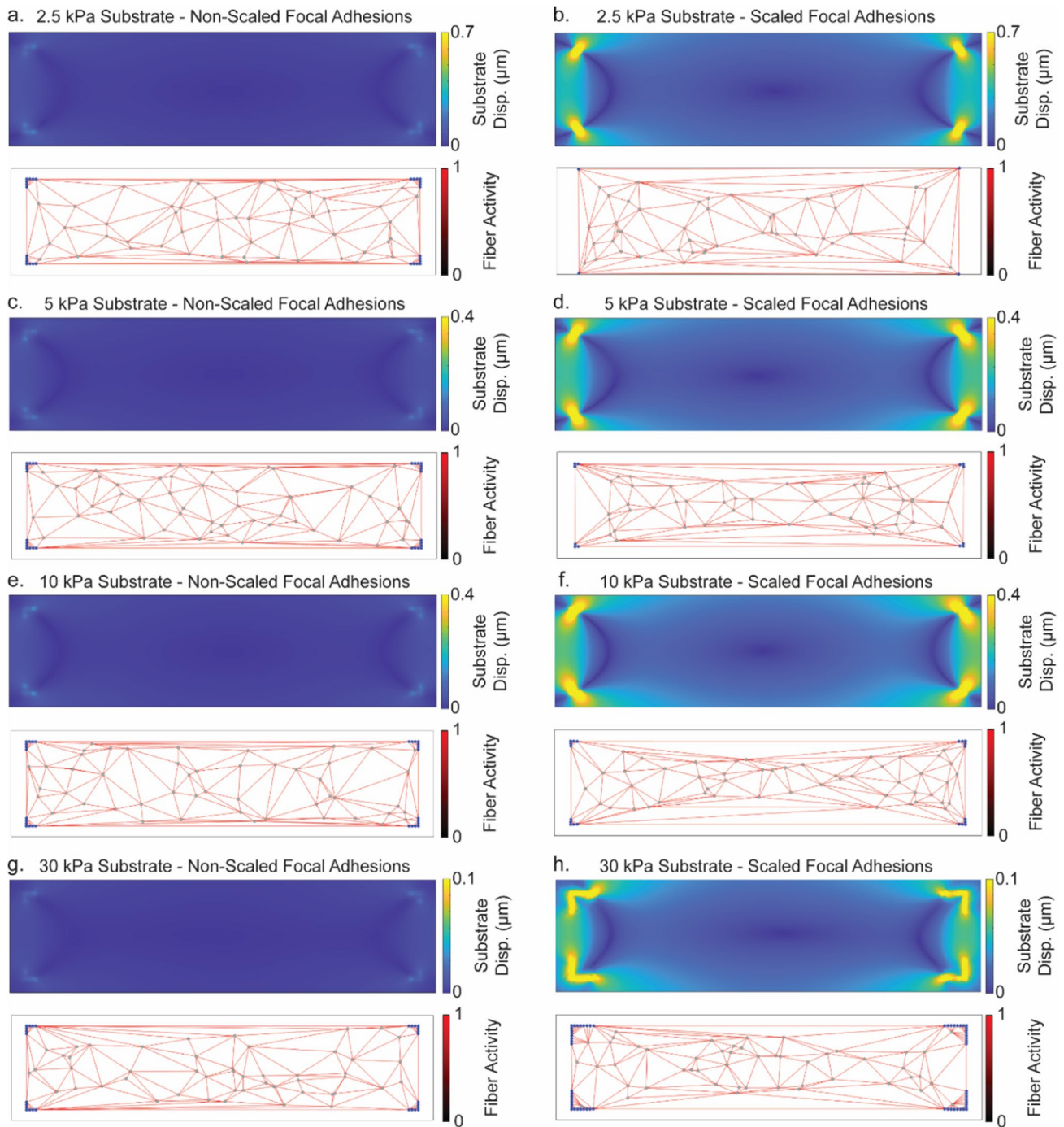
Fig. 10 Substrate deformation is more pronounced with substrate stiffness-dependent focal adhesion scaling. (**a.**, **c.**, **e.**, **g.**) Representative substrate displacement fields (top) and cytoskeletal networks (bottom) for the constant focal adhesion simulations on 2.5 kPa, 5 kPa, 10 kPa, and 30 kPa elastic substrates. (**b.**, **d.**, **f.**, **h.**) Representative substrate displacement fields (top) and cytoskeletal networks (bottom) for the scaled focal adhesion simulations on 2.5 kPa, 5 kPa, 10 kPa, and 30 kPa elastic substrates

connection laborious and very difficult. The impractical and perhaps impossible parameterization of VSMC biochemical signaling promotes the use of logic-based signaling networks as an alternative approach to gain insight on contractile force generation (Kraeutler et al. 2010; Irons and Humphrey 2020; Yoshida et al. 2022).

The current formulation of the model makes the simplifying assumption that the biochemical activation signal is uniform throughout the cell and does not explicitly
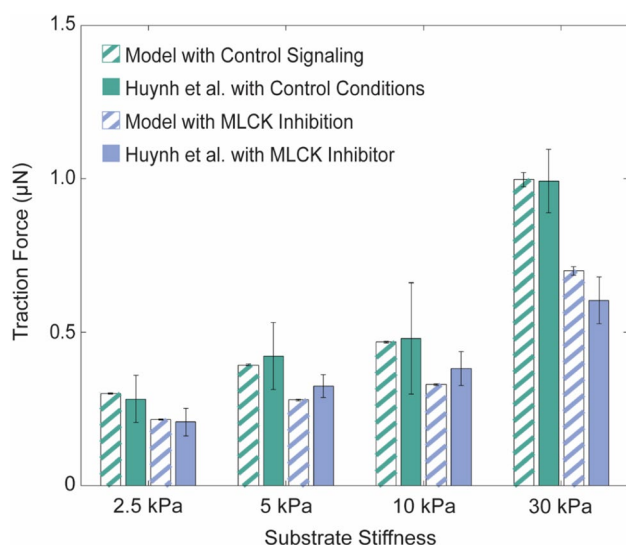
Fig. 11 Structural bio-chemo-mechanical model captures VSMC traction stress changes with increasing substrate stiffness coupled with MLCK inhibition. Steady-state traction force for scaling FA numbers in silico predictions and in vitro Huynh et al. experimental data with and without limitation of MLCK activity. The maximum tensile stress, σ_{max}, is scaled such that the in silico 2.5 kPa traction forces match the reported experimental value under control conditions. Error bars are SEM for $n = 12$

consider nuclear dynamics or intracellular transport. Some cell types, such as actively migrating VSMCs, exhibit varying degrees of polarity and intracellular signaling heterogeneity (Tang and Gerlach 2017). The non-motile form of VSMCs represented by the present form of the model, however, do not have a significant amount of signaling heterogeneity. Transport of signaling species could be introduced into the simulated VSMCs via the addition of a network of microtubules which would allow for the directional redistribution of intracellular components. A future area for potential application of the model is demonstrated by the crude way in which the SUN1 knockdown was modeled in the current study (through changes in RhoA rather than including SUN1 explicitly). SUN1/2 comprise the perinuclear space components of LINC complexes, acting similarly to cell–matrix adhesions but instead connecting the cytoskeleton and interior of the nucleus. Mechanotransduction between the nucleus and cytoskeleton are mediated mainly through the LINC complex of the nuclear membrane, and disruption of this complex has been demonstrated to affect cellular force generation, including VSMC contractility (Porter et al. 2020). While the importance of communication between the cytoskeleton and nucleus through LINC complexes is well established, the mechanisms behind the ensuing cellular responses remain an active point of research (Jones et al. 2022). Future iterations of the model could include a stiff

intracellular body, representative of a nucleus, and proposed nuclear-cytoskeletal mechanotransduction mechanisms could be evaluated in silico.

While the inclusion of a discrete fiber network allows for a detailed description of actomyosin stress fibers, the model does not account for the contributions from other cytoskeletal components such as microtubules and intermediate filaments. In many cell types, microtubules provide resistance to the compressive strain generated by actomyosin. The cooperativity of actomyosin and microtubules is described via the tensegrity model and gives rise to a proposed mechanism for cell shape maintenance and stability (Stamenović 2005). An exact mechanism describing the cooperativity between the force-generating actomyosin stress fibers and resisting microtubules, however, has yet to be identified and fully described. Additionally, much of the available work in this area is contradictory. While many agree that microtubule destabilization results in an increase in traction force generation (Zhang et al. 2000; Ahmed et al. 2022), there are conflicting reports on the role of stabilization with some reporting a decrease (Ahmed et al. 2022) in traction stress and others reporting no effect (Zhang et al. 2000) on force generation. The lack of a clear mechanism and consensus on the role of microtubule instability in VSMC contractility make it impractical to incorporate into a model. However, as the details on the role of microtubules become more apparent and defined, the model could easily be adapted to include an additional cytoskeletal component with a representative degree of mechanical instability.

The static nature of the focal adhesions and stress fibers in the current formulation of the model limits its capability in capturing VSMC mechanosensitivity fully. While the model does not currently allow for stress fibers nor focal adhesions to disassociate and re-form elsewhere, it is well established that cells exercise these processes to adapt to their environment (Balaban et al. 2001; Yeh et al. 2017; Trichet et al. 2012). Focal adhesions will preferentially form and mature in regions of high traction stress. For micropatterned cells, the high traction stress regions where focal adhesions form are localized in the corners (Fig. 3 of Ellefsen et al. 2019) and in the protrusions of non-micropatterned cells (Fig. 1 of Yeh et al. 2017). The stress fibers are then established to reinforce these focal adhesions and the cell body. The model limitations are most revealed in the need for manual adaptations to the initial VSMC geometry to capture geometric (Fig. 6) and stiffness (Fig. 9, 11)-dependent contractility changes. While the non-pre-aligned cytoskeletons did exhibit anisotropy in the more elongated geometries (Fig. 5a, c, e, g), the anisotropy did not approach the degree observed by Win et al. (Win et al. 2017) The non-pre-aligned cytoskeletons also became more aligned throughout the simulation due to the free nodes

shifting slightly to maintain mechanical equilibrium (Figure S2). The dynamic re-alignment, however, was limited since the stress fibers were not allowed to re-form to reinforce the cell as they would in vitro. The static nature of the modeled focal adhesions prevented the model from fully capturing the increased contractility observed on stiffer substrates, as well. While incorporating cytoskeletal and focal adhesion dynamics in future adaptations of the model will make it more representative of in vitro VSMC behavior, the need for their manual inclusion here reveals mechanisms that are difficult to observe experimentally. By uncoupling cytoskeletal anisotropy from cell geometry, the model demonstrates that the increase in contractility in elongated cells is a result of increased stress fiber anisotropy, not necessarily the shape itself. Additionally, through the control of focal adhesion number, the model further underscores the importance of focal adhesion mechanosensitivity and signaling in regulating VSMC contractility.

The inclusion of four interacting components makes the structural bio-chemo-mechanical model a comprehensive and broadly applicable simulation of in vitro VSMC TFM experiments. The model correctly predicts contractility changes observed with differential biochemical signaling, altered cell geometry, and varied substrate stiffnesses. While certain improvements could certainly be made, such as stress-responsive focal adhesion formation and more comprehensive biochemical signaling networks, the current formulation of the model provides a useful tool in bridging the gap between in silico predictions of VSMC behavior and in vitro experiments and has the potential to expand as more information becomes available. The prediction of the effects of long-term changes in VSMC signaling, such as that driven by hypertension, has remained elusive to arterial mechanobiologists. Thus, focusing in on short-term contractile behavior offers an interesting avenue to approach the problem. The wealth of published TFM experiments demonstrating the mechanosensitivity of VSMCs is a valuable resource and should be exploited to formulate these future short- and long-term models. The correct simulation of VSMC behavior under TFM experimental conditions can serve as a conduit to connect in vitro behavior to more complex in silico predictions, rendering the structural bio-chemo-mechanical model a promising resource for the future.

Declarations

References

Ahmed S, Johnson RT, Solanki R, Afewerki T, Wostear F, Warren DT (2022) Using polyacrylamide hydrogels to model physiological aortic stiffness reveals that microtubules are critical regulators of isolated smooth muscle cell morphology and contractility. Front Pharmacol 13(January):1–14. https://doi.org/10.3389/fphar.2022.836710

Balaban NQ, Schwarz US, Riveline D, Goichberg P, Tzur G, Sabanay I, Mahalu D et al (2001) Force and focal adhesion assembly: a close relationship studied using elastic micropatterned substrates. Nat Cell Biol 3(5):466–472

Brozovich FV, Nicholson CJ, Degen CV, Gao YZ, Aggarwal M, Morgan KG (2016) Mechanisms of vascular smooth muscle contraction and the basis for pharmacologic treatment of smooth muscle disorders. Pharmacolog Rev 68(2):476. https://doi.org/10.1124/pr.115.010652

Butler JP, Tolic-Norrelykke IM, Fabry B, Fredberg JJ (2001) Traction fields, moments, and strain energy that cells exert on their surroundings. Am J Physiol Cell Physiol 282:C595-605. https://doi.org/10.1152/ajpcell.00270.2001.-Adherent

Chen WW, Niepel M, Sorger PK (2010) Classic and contemporary approaches to modeling biochemical reactions. Genes Dev 24:1861–1875. https://doi.org/10.1101/gad.1945410

Deshpande VS, McMeeking RM, Evans AG (2006) A bio-chemo-mechanical model for cell contractility. Proc Natl Acad Sci 103(38):14015–14020

Dimitrije S (2005) Microtubules may harden or soften cells, depending of the extent of cell distension. J Biomech 38(8):1728. https://doi.org/10.1016/j.jbiomech.2004.07.016

Ellefsen KL, Holt JR, Chang AC, Nourse JL, Arulmoli J, Mekhdjian AH, Abuwarda H et al (2019) Myosin-II mediated traction forces evoke localized piezo1-dependent Ca^{2+} flickers. Commun Biol 2(1):298. https://doi.org/10.1038/s42003-019-0514-3

Estrada AC, Yoshida K, Saucerman JJ, Holmes JW (2021) A multiscale model of cardiac concentric hypertrophy incorporating both mechanical and hormonal drivers of growth. Biomech Model Mechanobiol 20(1):293–307. https://doi.org/10.1007/s10237-020-01385-6

Goffin JM, Pittet P, Csucs G, Lussi JW, Meister J-J, Hinz B (2006) Focal adhesion size controls tension-dependent recruitment of alpha-smooth muscle actin to stress fibers. J Cell Biol 172(2):259–268

Guglielmi G, Barry JD, Huber W, De Renzis S (2015) An optogenetic method to modulate cell contractility during tissue morphogenesis. Dev Cell 35(5):646–660. https://doi.org/10.1016/J.DEVCEL.2015.10.020

Hou JC, Shamsan GA, Anderson SM, McMahon MM, Tyler LP, Castle BT, Heussner RK et al (2019) Modeling distributed forces within cell adhesions of varying size on continuous substrates. Cytoskeleton 76(11–12):571–585. https://doi.org/10.1002/cm.21561

Huynh J, Bordeleau F, Kraning-Rush CM, Reinhart-King CA (2013) Substrate stiffness regulates PDGF-induced circular dorsal ruffle formation through MLCK. Cell Mol Bioeng 6(2):138–147. https://doi.org/10.1007/s12195-013-0278-7

Irons L, Humphrey JD (2020) Cell signaling model for arterial mechanobiology. PLoS Comput Biol 16(8):1–22. https://doi.org/10.1371/journal.pcbi.1008161

Irons L, Latorre M, Humphrey JD (2021) From transcript to tissue: multiscale modeling from cell signaling to matrix remodeling. Ann Biomed Eng 49(7):1701–1715. https://doi.org/10.1007/s10439-020-02713-8

Jones ML, Dahl KN, Lele TP, Conway DE, Shenoy V, Ghosh S, Szczesny SE (2022) The elephant in the cell: nuclear mechanics and mechanobiology. J Biomech Eng 144(8):1–9. https://doi.org/10.1115/1.4053797

Kraeutler MJ, Soltis AR, Saucerman JJ (2010) Modeling cardiac β-adrenergic signaling with normalized-hill differential equations: comparison with a biochemical model. BMC Syst Biol 4(157):157. https://doi.org/10.1186/1752-0509-4-157

Lang RJ, Tonta MA, Zoltkowski BZ, Meeker WF, Wendt I, Parkington HC (2006) Pyeloureteric peristalsis: role of atypical smooth muscle cells and interstitial cells of Cajal-like cells as pacemakers. J Physiol 576(3):695–705. https://doi.org/10.1113/JPHYSIOL.2006.116855

Menga N, Carbone G (2019) The surface displacements of an elastic half-space subjected to uniform tangential tractions applied on a circular area. Europ J Mech A/Solids 73(January):137–143. https://doi.org/10.1016/j.euromechsol.2018.07.011

Porter L, Minaisah RM, Ahmed S, Ali S, Norton R, Zhang Q, Ferraro E et al (2020) SUN1/2 are essential for RhoA/ROCK-regulated actomyosin activity in isolated vascular smooth muscle cells. Cells 9(1):132. https://doi.org/10.3390/cells9010132

Rausch M, Böhringer D, Steinmann M, Schubert DW, Schrüfer S, Mark C, Fabry B (2020) Measurement of skeletal muscle fiber contractility with high-speed traction microscopy. Biophys J 118(3):657–666. https://doi.org/10.1016/j.bpj.2019.12.014

Rensen SSM, Doevendans PAFM, Van Eys GJJM (2007) Regulation and characteristics of vascular smooth muscle cell phenotypic diversity. Neth Hear J 15(3):100–108. https://doi.org/10.1007/BF03085963

Ross J (1983) Cardiac function and myocardial contractility: a perspective. J Am Coll Cardiol 1(1):52–62. https://doi.org/10.1016/S0735-1097(83)80010-2

Saucerman JJ, Brunton LL, Michailova AP, McCulloch AD (2003) Modeling β-adrenergic control of cardiac myocyte contractility in silico. J Biol Chem 278(48):47997–48003. https://doi.org/10.1074/JBC.M308362200

Schwarz US, Soiné JRD (2015) Traction force microscopy on soft elastic substrates: a guide to recent computational advances. Biochim Et Biophys Acta Mol Cell Res 1853(11):3095–3104. https://doi.org/10.1016/j.bbamcr.2015.05.028

Seasholtz TM, Zhang T, Morissette MR, Howes AL, Yang AH, Brown JH (2001) Increased expression and activity of RhoA are associated with increased DNA synthesis and reduced P27kip1 expression in the vasculature of hypertensive rats. Circ Res 89(6):488–495. https://doi.org/10.1161/hh1801.096337

Singh K, Randhwa G, Salloum FN, Grider JR, Murthy KS (2021) Decreased smooth muscle function, peristaltic activity, and gastrointestinal transit in dystrophic (Mdx) mice. Neurogastroenterol Motil 33(e13968):1–10. https://doi.org/10.1111/nmo.13968

Sultan A, Warren DT (2018) Vascular smooth muscle cell contractile function and mechanotransduction. Vessel Plus 2(11):36. https://doi.org/10.20517/2574-1209.2018.51

Tang DD, Gerlach BD (2017) The roles and regulation of the actin cytoskeleton, intermediate filaments and microtubules in smooth muscle cell migration. Respir Res 18(54):1–12. https://doi.org/10.1186/S12931-017-0544-7

Trichet L, Le Digabel J, Hawkins RJ, Vedula SRK, Gupta M, Ribrault C, Hersen P, Voituriez R, Ladoux B (2012) Evidence of a large-scale mechanosensing mechanism for cellular adaptation to substrate stiffness. Proc Natl Acad Sci USA 109(18):6933–6938. https://doi.org/10.1073/pnas.1117810109

Uehata M, Ishizaki T, Satoh H, Ono T, Kawahara T, Morishita T, Tamakawa H et al (1997) Calcium sensitization of smooth muscle mediated by a rho-associated protein kinase in hypertension. Nature 389(6654):990–994. https://doi.org/10.1038/40187

Vedula SR, Krishna GP, Cheddadi I, Chen T, Brugués A, Hirata H, Lopez-Menendez H et al (2015) Mechanics of epithelial closure over non-adherent environments. Nat Commun. https://doi.org/10.1038/ncomms7111

Wen JH, Vincent LG, Alexander Fuhrmann Yu, Choi S, Hribar KC, Taylor-Weiner H, Chen S, Engler AJ (2014) Interplay of matrix stiffness and protein tethering in stem cell differentiation. Nat Mater 13(10):979–987. https://doi.org/10.1038/nmat4051

Yeh Y-C, Ling J-Y, Chen W-C, Lin H-H, Tang M-J (2017) Mechanotransduction of matrix stiffness in regulation of focal adhesion size and number: reciprocal regulation of caveolin-1 and B1 integrin. Nat Sci Rep 7:15008. https://doi.org/10.1038/s41598-017-14932-6

Yoshida K, Saucerman JJ, Holmes JW (2022) Multiscale model of heart growth during pregnancy: integrating mechanical and hormonal signaling. Biomech Model Mechanobiol 21:1267–1283. https://doi.org/10.1007/s10237-022-01589-y

Yuan SL, Lee EW, Zahra A, Park JH (2015) Risk factors of cardiovascular disease and their related socio-economical, environmental and health behavioral factors: focused on low-middle income countries-a narrative review article. Iran J Public Health 44(4):435

Zaw W, Buksa JM, Steucke KE, Gant Luxton GW, Barocas VH, Alford PW (2017) Cellular microbiaxial stretching to measure a single-cell strain energy density function. J Biomech Eng. doi 10(1115/1):4036440

Zhang D, Jin N, Rhoades RA, Yancey KW, Swartz DR (2000) Influence of microtubules on vascular smooth muscle contraction. J Muscle Res Cell Motil 21(3):293–300. https://doi.org/10.1023/A:1005600118157